Author Manuscript

Author Manuscript

Author Manuscript

Author Manuscript

HHS Public Access

Author manuscript

FEBS J. Author manuscript; available in PMC 2024 April 01.

Published in final edited form as:

FEBS J. 2023 April ; 290(7): 1822–1839. doi:10.1111/febs.16673.

APOBEC3G protects the genome of human cultured cells and mice from radiation-induced damage

Yelena Britan-Rosich[1,¶], **Jing Ma**[2,¶], **Eran Kotler**[3], **Faizan Hassan**[1], **Alexander Botvinnik**[1], **Yoav Smith**[4], **Ofra Moshel**[5], **Abed Nasereddin**[6], **Gunjan Sharma**[1], **Eli Pikarsky**[1], **Susan Ross**[2,*], **Moshe Kotler**[1,*]

[1.]Department of Pathology and Immunology, The Lautenberg Center for Immunology and Cancer Research, The Hebrew University Hadassah Medical School, Jerusalem, Israel.

[2.]Department of Microbiology and Immunology, College of Medicine, University of Illinois at Chicago, USA

[3.]Department of Genetics, Stanford University School of Medicine, Ca, USA

[4.]Genomic Data Analysis, Hadassah Medical School, Hebrew University, Jerusalem, Israel.

[5.]Core Research Facility, Institute for Drug Research, School of Pharmacy, Faculty of Medicine, The Hebrew University-Hadassah Medical School, Jerusalem, Israel

[6.]Core Research Facility of the Hebrew University-Hadassah Medical School, Jerusalem, Israel

Abstract

Cytosine deaminases AID/APOBEC proteins act as potent nucleic-acid editors, playing important roles in innate and adaptive immunity. However, the mutagenic effects of some of these proteins compromise genomic integrity and may promote tumorigenesis. Here, we demonstrate that human APOBEC3G (A3G), in addition to its role in innate immunity, promotes repair of double-strand breaks (DSBs) *in vitro* and *in vivo*. Transgenic mice expressing *A3G* successfully survived lethal irradiation, whereas wild-type controls quickly succumbed to radiation syndrome. Mass spectrometric analyses identified the differential up-regulation of a plethora of proteins involved in DSB repair pathways in *A3G*-expressing cells early following irradiation to facilitate repair. Importantly, we find that A3G not only accelerates DSB repair, but also promotes deamination-dependent error-free rejoining. These findings have two implications: (i) strategies aimed at inhibiting A3G may improve the efficacy of genotoxic therapies used to cure malignant tumors;

[*]To whom correspondence should be addressed: moshek@ekmd.huji.ac.il ; Tel: (972) 5054332176, srross@uic.edu.

[¶]J.M. and Y.B-R. Contributed equally to this work

Author contributions

JM and SR carried out and analyzed statistically all the experiments with the irradiated mice. YBR and EP performed the histological analysis. YBR, AB and GS carried out the experiments with the cultured cells including FACS, clonogenicity assay, transfections and maintaining. YS, FH and OM performed the Mass spectrometry analysis. GS and AN carried out the PCR amplification and the next generation sequencing. EK performed the statistical analysis of the NGS sequences. SR and MK conceptualized, designed and instructed the experiments. SR and MK supervised the research and analyzed the data. MK wrote the initial draft. YBR contributed to the discussion, and all authors contributed to the editing of the manuscript. YBR and JM contributed equally for this work.

Conflict of interest

The authors certify that they have NO affiliations with or involvement in any organization or entity with any financial interest or non-financial interest in the subject matter or materials discussed in this manuscript.

Author Manuscript Author Manuscript Author Manuscript Author Manuscript

and (ii) enhancing *A3G* activity may reduce acute radiation syndrome in individuals exposed to ionizing radiation.

Graphical Abstract

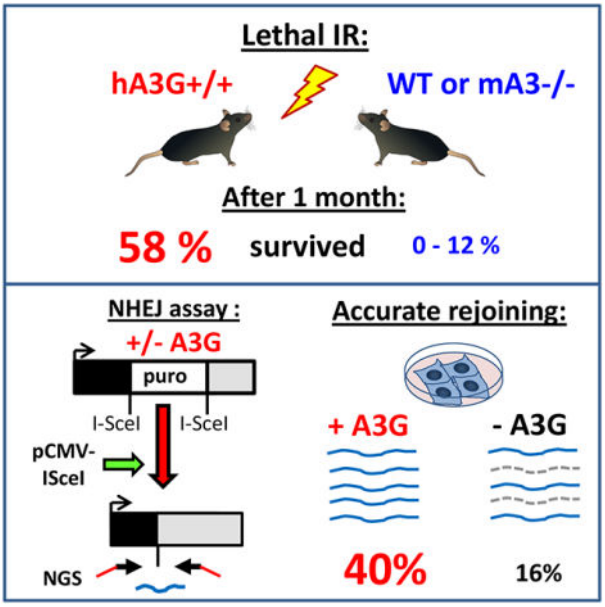

A3G protects mice from IR-induced damage and promotes accurate DNA double-strand breaks repair in cultured cells. Transgenic mice expressing A3G successfully survived lethal irradiation, whereas wild type controls quickly succumbed to radiation syndrome. In cultured cells, A3G accelerates DSB repair and promotes survival of cells after irradiation. Moreover, in a cell-based non-homologous end-joining reporter system A3G promotes deamination-dependent error-free rejoining of the induced double-strand break mediated by I-SceI.

Keywords

cytidine deaminase; APOBEC3G; DNA damage response; DNA repair; homologous recombination; non-homologous end joining; mouse

Introduction

The human activation-induced cytidine deaminases (AID) A1, A2 and A4, and apolipoprotein B mRNA-editing enzyme-catalytic polypeptide-like (APOBEC) proteins are members of a multifunctional family of Zn^{2+}-dependent polynucleotide cytosine deaminases (CDs) that act as potent editors of single-stranded DNA (ssDNA) and RNA [1–3]. Proteins of the AID/APOBEC family are expressed in all vertebrates and modulate both acquired and innate immune responses by cytosine to uridine (C>U) deamination of the hosts' or the pathogens' genomes [3–6].

The evolutionarily conserved AID/APOBEC1 locus is considered to be the ancestral gene of the AID/APOBEC family in vertebrates. It encodes for the AID protein [3, 6–8],

Author Manuscript Author Manuscript Author Manuscript Author Manuscript

which plays a pivotal role in the adaptive immune system by editing deoxycytosines in immunoglobulin genes (Ig), triggering somatic hypermutation (SH) and class-switch recombination (CSR). Hence, AID fulfills an essential pro-mutagenic function in the generation of diverse and efficient antibodies [6]. However, AID is not the only human APOBEC protein involved in chromosomal DNA editing and mutagenesis. In many tumors APOBEC-induced mutation-signatures have been identified [9–13]. For instance, accumulation of TC>TT (and consequently GA>AA) substitutions were revealed in breast cancer, head-and-neck squamous cell carcinomas and in HPV-associated cervical carcinomas [9, 14–20], concomitant with high levels of expression of A3A and A3B [19–21]. Furthermore, extensive sequencing efforts revealed that the genomes of many cancers contain hyper-mutated regions termed *kataegis* [9–13]. Base substitutions within these disrupted regions are mostly of cytosine in TpC dinucleotides and are closely associated with regions of genomic re-arrangements. The latter often occur on the same chromosomal strand over long genomic distances, suggesting that deaminases act simultaneously and/or in a processive manner over a limited time period [9–12]. Furthermore, short tandem repeats, or short stretches of identical sequences at the breakpoints (overlapping microhomology) commonly flank insertions/deletions (INDELs) in such regions [11, 12, 22].

In mammals, the APOBEC3 (A3) proteins exhibit broad restriction activities against retrotransposons and retroviruses by deamination-dependent and -independent mechanisms [4, 23–27]. Recently, similar CDs involved in innate immunity have been described in invertebrate species, suggesting that these genes likely emerged long before the appearance of vertebrates [28]. The early emergence and the broad evolutionary distribution of AID/APOBEC-like genes strongly suggest that these proteins play important biological roles in innate and adaptive immune systems. It thus becomes clear that the pro-mutagenic functions of AID/APOBEC proteins may act as a double-edge sword and must be tightly regulated to enhance immunity, while avoiding the disruption of genomic integrity, DNA hypermutation and promiscuous RNA/DNA editing, which could promote tumorigenesis [9, 12, 19–21, 29].

Interestingly, while mice express only the A1, A2 and a single A3 (mA3) proteins the human genome encodes for seven additional homologous CD proteins of the A3 family designated A3A, B, C, DE, F, G and H. All seven human A3 members are encoded within the *APOBEC3* locus on chromosome 22 [1–4], exemplifying the evolutionary diversification in deamination activity or functionality. In line with this expansion, A3 proteins have been implicated in specific functions. For example, human A3G prevents emergence of retroelements [4, 25]; A3F, A3G and A3H neutralize Vif-deficient HIV-1 by editing ssDNA reverse transcripts [4]; A3A has been implicated in mitochondrial DNA mutagenesis, demethylation of 5-methylcytosine in genomic DNA, induction of DNA breaks in a deaminase-dependent manner [30–33], clearance of foreign DNA from cells [34], RNA editing [35, 36] and protection against DNA viruses [21, 37, 38]. It was recently shown that A3A promotes polyp and tumor formation in transgenic APC^{min} mice, likely through increasing cytidine deamination of genomic DNA and subsequent loss of heterozygosity of the wild type allele [23].

Intriguingly, diffuse large B-cell lymphoma (DLBCL), several glioblastoma, lung adenocarcinoma and pancreatic cancer cell lines expressing high levels of A3G are resistant

Author Manuscript Author Manuscript Author Manuscript Author Manuscript

to chemo- and radio- therapies [39–42], suggesting additional roles for A3G. We have previously shown that cells expressing endogenous A3G are highly resistant to ionizing radiation (IR) compared to cells devoid of A3G [39, 43]. Moreover, A3G is recruited to DSB repair foci and knock down of A3G or inhibition of A3G by peptides convert radio-resistant cells to radio-sensitive [43]. These data further provide a substantial evidence to assume that A3G is involved in DSB repair.

Here we demonstrate that A3G acts as a radio-protective agent that promotes DSB repair in cultured cells and rescues mice from lethal dose of IR. We show that in human cells subjected to a single DNA double-strand break, wild type (wt) A3G promotes accurate break repair, significantly reducing mutation error rates. Consistently, expression of human A3G in mice lacking the expression of mA3 reduces the damage to liver and spleen caused by lethal IR doses, preventing acute radiation syndrome and enabling recovery. These results, along with our previous findings that KD and inhibition of A3G convert radio-resistant cells to radio-sensitive, provide a plausible explanation to the reduced sensitivity of A3G-overexpressing tumors to genotoxic therapies and have important implications for the treatment of such tumors by combinatorial targeting of A3G, as well as for the prevention and treatment of severe radiation effects.

Results

A3G promotes the repair of DSBs induced by IR in cultured cells

To examine the effects of A3G expression on genotoxic stress-induced DSB repair, we first subjected the following cells to IR (3Gy): Human embryonic kidney (HEK293), SupT11^{EV} (acute lymphoblastic leukemia T-cells transfected with empty vector [44]) and the leukemic SupT1 cells, which do not express A3G, as well as their counterparts which express recombinant A3G : HEK293-A3G, SupT11^{A3G}, as well as the endogenous A3G-expressing lymphoma H9 cells.

The repair-kinetics of the DSBs induced by IR was determined along 24-hours post IR by staining the cells with anti-γH2AX followed by flow cytometric analysis (Fig 1A). While the A3G-expressing and non-expressing cells exhibited similar levels of damage shortly after IR exposure, a significant reduction in the percentage of γH2AX-positive cells was observed only in the A3G-expressing cells, particularly at 24-hours post-IR. DSBs were still visible in 62% of non-A3G expressing controls, compared to only 11% in HEK293-A3G cells ($p=0.026$), (Fig. 1A, left panel). Similarly, the SupT11^{A3G} cells recovered more efficiently than the control SupT11^{EV} cells ($p=0.02$, $p=0.014$, $p=0.03$, for 4h, 8h and 24h time points, respectively) (Fig. 1A, middle panel). The A3G-expressing lymphoma H9 cells efficiently repaired the IR-induced DSBs comparing to the A3G-devoid leukemia SupT1 cells (Fig. 1A, right panel). These results indicate that recombinant A3G as well as the endogenous A3G expressed in lymphoma cells promotes DSB repair, supporting our previous reports [39, 43, 45]

To test the impact of A3G protein on cells survival following IR-exposure, we performed clonogenic experiments using HeLa and HeLa-A3G cells. In parallel, the same HeLa-A3G and HeLa cells were irradiated (4Gy) and cells were collected for γH2AX analysis at time

Author Manuscript Author Manuscript Author Manuscript Author Manuscript

intervals through 24 hours post irradiation (Fig. 1B and C). Small numbers of cells (10^2, 3×10^2 and 10^3) were seeded in 6-well plates, and 3 hours later following cells adherance they were irradiated at 2 and 4 Gy. Seven days post irradiation colonies of >20 cells (over 4 divisions) were counted. The survival rate was calculated as the ratio between the number of colonies at each irradiation dose and the number of colonies emerged from non-irradiated cells (Fig. 1C). Plotting the ratio between the number of colonies developed without exposure to those developed after irradiation reveals that the expression of A3G in HeLa cells increases the relative survival rate of colonies formation by 1.9-folds and 4-folds at 2 Gy and 4 Gy respectively (p=0.01, p=0.006, respectively) (Fig. 1D). These findings point at a tight correlation between the increased survival rate and the reduction in numbers of cells stained with γH2AX shortly after IR exposure (Fig. 1B–D).

Taken together, we confirmed that expression of A3G promotes the DSB repair and increases the survival rate of cultured cells. Our efforts to find whether A3A, A3B, A3C and A3F proteins promote DSBs repair failed so far. Expression of A3A protein in HEK293 caused large number of DSBs leading to early cells death post IR (results are not shown), as reported previously [46].

A3G promotes the repair of DSBs induced by IR *in vivo*

We next thought to examine the effects of A3G on DSB repair *in vivo*. To this end, we used two strains of mA3 knockout transgenic mice (mA3−/−) which express a myc-tagged human A3G under the control of the chicken β-actin promoter [47, 48] at either high ($A3G^{high}$) or low ($A3G^{low}$) levels. Of note, the levels of A3G expression in peripheral blood mononuclear cells (PBMCs) of $A3G^{high}$ mice are similar to A3G levels in human PBMCs, and are approximately 30-fold higher than in the $A3G^{low}$ strain [47]. Untreated wild type (mA3+/+) and mA3 knockout (mA3−/−) [49] mice were used as controls. These mice (12–17 mice/group) were exposed to a whole-body lethal dose of IR (8.25 Gy) [50] in three independent experiments, and their survival was recorded for 30 days post-irradiation. Expectedly, nearly all of mA3+/+ and most of mA3−/− mice succumbed to irradiation (0% and 12% of these mice survived, respectively). In contrast, 58% of $A3G^{high}$ and 45% of $A3G^{low}$ mice survived this high IR dose (Fig. 2A, p=0.0136 for $A3G^{High}$ *vs* mA3−/− and p=0.0547 for $A3G^{Low}$ *vs* mA3−/−). Clinically, IR-susceptible mA3+/+ and mA3−/− mice rapidly lost weight post-IR and suffered from severe anemia while IR survivors from the $A3G^{high}$ strain successfully recovered and gained weight by day 30 of the experiment (Fig. 2B–E). All the mice that survived to 30 days rebounded to normal levels in weight (Fig. 2B), white blood cells (Fig. 2C), red blood cells (Fig. 2D) and hemoglobin (Fig. 2E) (compare day 0, day 12 and day 30 values).

A3G prevents liver necrosis and promotes splenic recovery in irradiated mice

We next turned to evaluate the clinical and pathological outcomes of the above IR dosages across the genotypic groups. Histological examination of spleens and livers derived from mA3−/− and mA3+/+ mice showed massive cell depletion, which is the hallmark of radiation syndrome (Fig. 3). In contrast, livers and spleens taken from $A3G^{high}$ mice, which survived the entire 30 days of the experiment showed normal morphology and no or little tissue damage, suggesting that they recovered from the damage caused by radiation (Fig.

Author Manuscript Author Manuscript Author Manuscript Author Manuscript

3A). Numerous necrotic foci were observed in the livers of irradiated knockout (mA3−/−) mice, while the liver sections prepared from irradiated wild type (mA3+/+) and transgenic $A3G^{high}$ mice were free of necrosis (Fig. 3A, upper panel; 3B–i). Similarly, spleens of wild type and knockout mice, which did not recover from IR exhibited massive cell depletion, red and white pulp atrophy and hemorrhage-associated focal hemosiderin deposits (Fig. 3A, lower panel; 3B–ii), whereas those of surviving mice contained numerous foci of hematopoietic regeneration in the red pulp regions.

Intensive recovery was observed in A3G-expressing mice; all $A3G^{high}$ and $A3G^{low}$ (not shown) mice that survived 30 days post-IR showed complete recovery of spleen tissues accompanied by extensive extra-medullary hematopoiesis (compare with non-irradiated wild type control spleen in 3B-iii and iv).

Evidently, the spleens of the irradiated knockout mA3−/− mice contained foci of hyperplasia on a background of anemia and tissue atrophy, while the spleens of mA3+/+ mice showed massive depletion of red and white pulps, anemia and general organ atrophy. We thus attempted to characterize the cells that occupied hyper-proliferative splenic regions by staining for T- and B-cell specific markers (CD3 and CD45R, respectively) and for c-Kit, which is a hallmark of ongoing hematopoiesis. While specific signals were observed in other areas in the spleen, none of the hyperplastic regions were stained by these antibodies: CD3- and CD45R-positive cells reside in the lymphoid nodules at the white pulp regions whereas c-Kit staining was intensively distributed through the red pulp regions in the spleens of transgenic A3G mice, as well as in the spleens of all other mice groups (Fig. 3C). Thus, we characterized the induced hyperplasia as non-T, -B and non-c-Kit positive, but the origin of these hyper-proliferative regions remains to be elucidated.

Accurate DSB rejoining by A3G is deamination-dependent.

We next thought to examine how A3G affects DSB repair. To this end we induced single DSB in a stably-transfected exogenous plasmid bearing the ISce1 restriction-enzyme site in A3G-deficient cells (naïve HEK293), A3G-expressing cells (HEK293-A3G) as well as in cells expressing deamination-defective mutants (HEK293-A3G-W285A and HEK293-A3G-E259Q) [25, 51]. Briefly, cells were first stably transfected with a pimEJ5GFP (EJ5) plasmid which contains the ISceI restriction target site [52]. Then, to induce DSBs, cell cultures were transiently transfected with pCMV-NLS-ISceI plasmid expressing I-SceI restriction enzyme, an 18bp homing endonuclease (Fig. 4A). To examine the effects of A3G on the mode of repair of the DSB, we PCR-amplified and sequenced the ~131bp amplicon surrounding the rejoined ISceI site which consists exclusively of the rejoined fragments (see Methods). Sequencing reads (10^5 - 10^6 reads per sample, Table 1, Fig. S1) were aligned to the original plasmid sequence and the fractions of accurately repaired cleavage sites (18 bp) and of full-length (131bp) error-free amplicons were assessed.

Interestingly, the ratio between accurately restored (18bp long) ISceI site to the total sequences (accurate + inaccurate) in DNA derived from HEK293-A3G cells was ~2.2-fold higher ($p=0.00102$) than in A3G-deficient control cells, or from cells expressing deamination defective mutants ($p=0.067$ and $p=0.07$ for the W285A and E259Q mutants, respectively) (Fig. 4B). Similarly, quantification of the fraction of accurately restored

Author Manuscript Author Manuscript Author Manuscript Author Manuscript

sequences over the entire 131 bp fragment showed a ~2.7-fold improvement in wt-A3G-expressing cells comparing to naïve HEK293 (p=0.0152) or to the deamination-defective mutants (p=0.0155 and p=0.022 for the W285A and E259Q mutants, respectively). These results indicate that A3G significantly increases the accurate rejoining of cleavage sites, without inducing excessive mutations in the regions up/down-stream of the DSB site (including C to T or G to A transitions). Furthermore, since wt-A3G and the deamination-defective W285A and E259Q mutants were expressed at similar levels (Fig. 4C), the observed effects were attributed mainly to the deamination activity of the enzyme, indicating that the C-terminal catalytic domain of A3G is essential for promotion of DSB repair.

RNA binding to A3G is not essential for its DSB repair activity

At the structural level, the A3G protein contains two domains through which it may bind RNA and DNA [1–3, 53]. We and others have previously shown that treatment of purified A3G with RNase elevates its enzymatic deamination activity *in vitro* [54–56]. We therefore asked whether RNA binding affects A3G's ability to promote the repair of DSBs induced by IR. To this end, we irradiated (3Gy) HEK293, HEK293-A3G cells, and HEK293 expressing W94A and W127A A3G mutants and measured the kinetics of DSBs repair following IR (3Gy). These mutants lack RNA binding, yet they retain the ability to bind ssDNA and deaminate cytosines [53]. Examination of the fraction of cells retaining DSBs in a 24-hour time course following IR shows similar repair kinetics in cells expressing either W94A or W127A mutants to those observed in wt A3G expressing cells (Fig. 4D–E). These results indicate that binding of RNA molecules by A3G is not essential for its promotion of DSB repair.

Expression of A3G is associated with accumulation of DNA damage repair proteins post irradiation

We next thought to examine how A3G mediates repair in response to IR. Therefore, we compared the proteomes of A3G-expressing cells ($SupT11^{A3G}$) with that of A3G-deficient controls ($SupT11^{EV}$) before and at 3 and 8 hours post-IR using mass spectrometry (MS).

First, we verified the expression of A3G in irradiated $SupT11^{A3G}$ cells through the course of 24 hours of the experiment by detection of A3G signal in the MS data. The A3G signals observed in $SupT11^{EV}$ cells represent the background of the system (Fig. 5A). Then, to examine global trends within the data, we performed principal components analysis (PCA), projecting the raw MS data into low dimensional space where the distance between points represents the difference in expression levels (of all proteins) among the time-point samples (Fig. 5B). PCA analysis was performed at time points 0, 3 and 8 hours following radiation in $SupT11^{A3G}$ cells (blue balls) and $SupT11^{EV}$ cells (red balls). The PCA domain provides a statistical measurement independent from the group average. The longer the distance between balls (representing different time points), the greater the change in quantity of proteins in this time duration. The separation between the two groups is evident by the clear distance in axis PC#1 and PC#2 between the red balls and the blue balls. The distance between time points 0 and 3 hours in the $SupT11^{A3G}$ cells (blue balls group) is significantly larger than in the $SupT11^{EV}$ cells (red balls group). A major change in the quantity of proteins is occurring in the first 3 hours in $SupT11^{A3G}$ and not in $SupT11^{EV}$ cells.

Author Manuscript Author Manuscript Author Manuscript Author Manuscript

This analysis revealed an A3G-dependent difference between cellular proteomes already at baseline, which increases over time following IR. Furthermore, the overall proteomic change in A3G-expressing cells vs A3G-devoid cells early after IR (the distance ratio between projections of time points 0 to 3 hours) is about 3 vs 9 in the eigenvector domain suggesting that A3G expression is associated with defined cellular response/s to DNA damage.

To identify proteins that exclusively accumulated in A3G-positive cells, we first filtered out those that exhibited similar dynamic patterns in both cell lines over time by requiring a low correlation between them (Pearson $R<0.4$). Then, we selected proteins, which increased by at least 0.4-fold from 0 to 3 hours post IR and have not decreased during the next time interval (3 to 8 hours). This selection yielded a list of 279 proteins (listed in supplement Table S1), which we analyzed using the Search Tool for the Retrieval of Interacting Proteins (STRING) protein database. The STRING map (Fig. 5C) identifies the most significantly enriched KEGG pathway was HSA 03440-Homologous Recombination (HR), highlighting its key proteins including BLM, NBN, RAD50, RAD51C, RAD54B, TOP3A and TOPBP1. In addition, Table 2 summarizes the pathway involvement of the most significantly expressed proteins chosen by the STRING and REACTOME Databases.

Furthermore, the most significantly enriched proteins that were expressed in SupT11^{A3G} cells immediately following IR are related to HR, NHEJ and NER, for example: Homology Directed Repair (HDR) through Single Strand Annealing (SSA) with BLM, ERCC1, ERCC4, KAT5, NBN, RAD50, TOP3A, TOPBP1 [HSA-5685938]; DNA Double-Strand Break Repair with BLM, CCNA2, ERCC1, ERCC4, EYA3, KAT5, NBN, PARP1, RAD50, RAD51C, TOP3A, TOPBP1, XRCC4 [HSA-5693532]; SUMOylation of DNA damage response and repair proteins with AAAS, BLM, NDNL2, NSMCE1, NSMCE4A, NUP107, PARP1, SMC6, XRCC4 [HSA-3108214]. Together, these results pose A3G as a mediator of the DSB response, which is associated with protein-level induction of DNA damage repair genes and promotes accurate end-joining upon DSB induction.

Discussion

In contrast to previous reports that linked deaminase activity of A3A and A3B to their hyper-mutagenic effect in tumor cells, here we show that A3G, in addition to its role in innate immunity, is involved in restoring cellular genome integrity rather than causing harmful mutagenesis. Certainly, the involvement of A3G, F and H proteins in the inhibition of retro-element propagation is an additional important way by which these proteins protect the host's genome integrity, as exemplified by A3G's *in vivo* anti-retroviral activity [23, 57]. The fact that several normal tissues [58] and some genotoxic-resistant tumors express high amounts of A3G [39–42] led us to ask whether A3G supports the survival of cells and mice from genotoxic treatments, such as IR. To address this question, we utilized both cellular models and transgenic mice strains to demonstrate the pivotal role of A3G in promoting DSB repair. *In vitro* A3G expression enabled efficient DSB repair while the absence of A3G increased radio-sensitivity. *In vivo*, we used two novel A3G transgenic mouse models expressing different levels of the human A3G transgene on a mA3-deficient background. Subjecting these mice to lethal IR doses exemplified the importance of A3G for genome recovery. The recovered A3G-expressing mice had normal-sized organs and morphology,

Author Manuscript Author Manuscript Author Manuscript Author Manuscript

with intensive extramedullary hematopoiesis in their spleens. Histological examination of the mouse organs, their body weight and blood counts showed that the A3G transgenic mice surviving to 30 days of the experiment successfully recovered from the IR syndrome. In contrast, all the WT and 88% of the mA3-knockout mice died or were euthanized prior to the end of the experiment. The findings recently reported by Tong and his coworkers [41] showing that inhibition of A3G radio-sensitizes A3G-expressing tumor cells, provide a solid support to our data presented here and in our previous publications [39, 43].

Further examination of A3G-mediated DSB repair activity showed that not only does A3G accelerate the rejoining, but it also promotes an error-free product. Strikingly, we found that deamination-active, but not inactive A3G, promotes accurate repair of DSBs generated by ISceI digestion. These results are surprising, since A3 proteins are DNA editors, which mutate CT>TT in ssDNA. Note, that while FACS analyses of irradiated cells (Fig. 1A–B) inform about the relative fractions of cells with DSBs remaining post IR, the results shown in Figure 4 depict the mode of DNA restoration following the rejoining of a specific type of DSB - the ISceI cleavage. While IR induces multiple DSBs, our measurements are limited by design to capture specific NHEJ of chromosomal DSB generated at the ISceI cleavage site.

Formation of short or long over-hanging ssDNA, which are generated during DSB repair, determines whether the DSB repair will proceed via NHEJ, HR or SSA pathways [52, 59, 60]. Our experiments were designed to examine the NHEJ pathway, which is responsible for the majority of cellular DSBs repair [52, 60]. Our test is not able to reveal the DSBs repaired via the HR, which restores the original sequences, or SSA pathway, which is mutation-prone and accomplished by generation of long deletions [52]. Our results show that A3G promotes error-free NHEJ (Fig. 4).

Accurate-NHEJ and HR are the two DSB repair pathways which restore the original sequence of the breakage sites. It was previously shown using atomic force microscopy that A3G multimers attach to ssDNA termini [39]. Interaction between such pairs of 3’ssDNA-A3G complexes generated at both ssDNA termini allows efficient elongation of the DNA on a template of the homologous strand. This notion is supported by: i) *in vitro* experiments showing that in the presence of A3G, Klenow fragment DNA polymerase accomplishes the synthesis of both DNA strands containing minimal homology of two bases [39, 61]; ii) A3G undergoes inter-segmental transfer [56, 62], allowing it to directly juxtapose two ssDNA termini with minimal terminal microhomology leading to error-free NHEJ and if juxtaposes along the resected ssDNA it will generate error prone-NHEJ. Others and we showed that A3G, albeit its predominant cytoplasmic protein, can translocate, reside and act in the nuclei [25, 39, 45, 63–66] pointing at its potential to interact with damaged DNA in the cell genome.

We suggest therefore that A3G is involved in two activities: i) Deamination-active A3G promotes the removal of the ssDNA tails through induction of the dU excision; ii) A3G molecules bound to the 3’ssDNA termini at the DSB site stimulate fast and efficient end joining and support accurate DSB repair. These two A3G functions act simultaneously to promote DSB repair.

Author Manuscript Author Manuscript Author Manuscript Author Manuscript

These putative A3G functions are also fulfilled by other cellular proteins. The Ku70–80 complex, like A3G, binds ssDNA preserving the sequence at the ssDNA termini and promoting NHEJ repair pathway [60, 67]. Both, Ku70–80 complex and A3G have to be removed to accomplish the ligation by DNA-PKcs, Artemis, XRCC4/LIG4, Pol λ ,Pol μ and Rev1 [60]. During the single-strand annealing, the ERCC1-XPF complex removes the over-hanging ssDNA generated during DSB repair, similar to the putative function of A3G. The ERCC1-XPF complex is a structure-specific endonuclease, which is involved in removing the non-homologous tails during DSB repair by cleaving the DNA on the 5’ strand, at a distance of two nucleotides from the ds/ssDNA junction [68–71]. *In vitro* studies showed that stem/loop structures are used as substrates for A3G and ERCC1/XPF complexes, suggesting that both proteins directly catalyze ssDNA, without involvement of other cellular factors. The ERCC1/XPF complex catalyzes short ssDNA regions of at least 6 nucleotides in a loop structure, whereas A3G deaminates 5’CC→CU at the ssDNA termini, close to the double-strand junction and also in the loop context [61], triggering single-strand nicking upon recruitment of uracil DNA-glycosylase activity [72–74]. Since both A3G and the ERCC1/XPF complex promote similar biochemical outcomes, we suggest that A3G, like the ERCC1/XPF complex, participates in the removal of the ssDNA tails generated during genomic DNA repair [75].

In summary, the results presented in this report demonstrate that A3G molecules rescue cells and mice from the deleterious effect of DSBs induced by genotoxic agents (such as IR) by promoting DSB repair. Thus, A3G in addition to its role in innate-immunity plays a key role in preserving genomic integrity. DSBs are among the most deleterious types of DNA lesions that if not repaired, can lead to cell death. Our results point to A3G as a novel drug target for circumventing tumor resistance to chemo- and radio-therapies; inhibiting A3G expression or its deaminase catalytic activity may improve the efficacy of genotoxic therapies for cancer. Furthermore, enhancing A3G function could improve the outcomes of exposure to irradiation, either accidentally or due to non-conventional terrorism.

Materials and Methods

Ethics statement

All mice were housed according to the policies of the Institutional Animal Care and Use Committee of the Animal Care Committee (ACC) of the University of Illinois at Chicago (UIC). All studies were performed in accordance with the recommendations in the *Guide for the Care and Use of Laboratory Animals* of the National Institutes of Health (National Research Council. 1996 in [57]. These committees approved the experiments performed with mice in this study (UIC ACC protocol 18–168).

Mice

All mice were bred at the University of Illinois at Chicago. mA3+/+ and mA3−/− mice were previously described [49]. The two A3G transgenic mice strains expressing high ($A3G^{high}$) and low ($A3G^{low}$) levels of the transgene on the mA3−/− background were previously described [48] . Both transgenes are carried by heterozygous animals and non-transgenic mA3−/− mice used in the experiments were generated from the same cross. One month

Author Manuscript Author Manuscript Author Manuscript Author Manuscript

old mice were whole body irradiated with 8.25 Gy [50] and maintained for 30 days after irradiation, at which time all surviving mice were euthanized. Both female and male mice were included in the experiments.

Cells

T-acute lymphoblastic leukemia cells expressing A3G protein (SupT11^{A3G}) and their counterparts containing empty vector (SupT11^{EV}) were provided by Dr. R. S. Harris [44] (Department of Biochemistry, Molecular Biology and Biophysics, Institute for Molecular Virology, University of Minnesota, Minneapolis, MN 55455). SupT1, H9, HEK293-A3G, HeLa and HeLa-A3G cells were provided by the National Institutes of Health AIDS Research and Reference Reagent Program (AIDSP; Division of AIDS, National Institute of Allergy and Infectious Diseases, National Institutes of Health).

HEK293, HEK293-A3G, HeLa and HeLa-A3G cells were grown in DMEM, while H9, SupT1 and SupT11 cells were maintained in RPMI-1640. Cell culture media were supplemented with 10% fetal bovine serum, 100 U/ml, penicillin, 100 U/ml streptomycin, and 2 mM of L-glutamine (Biological Industries, Beit Haemek, Israel). A3G-expressing HEK293 and HeLa cells were maintained in the presence of G418 (at concentration of 0.5 mg/ml and 0.4 mg/ml, respectively). Expression of A3G was validated by RT-PCR and Western blot. Absence of mycoplasma infection was routinely confirmed by using EZ-PCR mycoplasma detection kit (Biological Industries, Beit Haemek, Israel).

Plasmids

Naïve HEK293 cells were stably transfected by standard Calcium Phosphate method with pFLAG-A3G plasmids carrying the A3G mutants W94A and W127A (provided by Dr. Marc-André Langlois, Faculty of Medicine, University of Ottawa, Canada) and pCDNA3.1-A3G-MycHis$_6$ bearing W285A or E259Q mutations (kindly provided by R.S.Harris). Following the transfection, cells were grown in the presence of 1mg/ml of G418 to select the A3G-expressing cells.

pimEJ5GFP (EJ5) was a gift from Jeremy Stark (Addgene plasmid #44026; http://n2t.net/addgene:44026; RRID: Addgene_44026) [52]. Naïve HEK293, HEK293-A3G, HEK-A3G-W285A and HEK-A3G-E259Q cells were transfected with EJ5 with Lipofectamine as previously described by Weinstock et al. [59]. Following transfection with EJ5, cultures were maintained for at least 14 days in medium containing puromycin (see scheme in Fig.4) to select cells stably containing the EJ5 reporter. pCMV-NLS-I-SceI plasmid expressing I-SceI endonuclease vector was generously provided by Dr. Ayub Nabieh [76], which was transfected into HEK293, HEK293-A3G and two deamination impaired mutants (W285A and E259Q) by using Lipofectamine as described above.

Radiation

Cells were irradiated by using the X-RAD 225 irradiator (Precision X-Ray), in tissue culture plates one day following passage the cells.

Author Manuscript Author Manuscript Author Manuscript Author Manuscript

Histological analysis

For histological analysis, spleens and livers were fixed and stored in 4% buffered formaldehyde for 48h, transferred to 80% ethanol and then embedded in paraffin. Five-micrometer tissue sections were stained with hematoxylin and eosin (H&E). Immunohistochemistry analyses were performed with antibodies against CD3 (Bio-Rad, USA), CD45R (R&D systems, USA) and c-Kit (Abcam) antigens.

Immunoblotting

Cell pellets were washed with PBS, lysed in Laemmli sample buffer (Sigma) and heated at 95°C for 10 min. Equivalent amounts of protein extracts were analyzed by 12% SDS/PAGE, followed by transfer of the proteins to poly (vinylidene difluoride) membrane. A3G protein was detected by using rabbit anti-A3G C-terminal-specific polyclonal antiserum (provided by the National Institutes of Health (NIH) AIDS Reagent Program (Division of AIDS, National Institute of Allergy and Infectious Diseases, NIH, USA) and secondary goat anti-rabbit horseradish peroxidase-conjugated antibody (Sigma), following blocking the membranes with Tris-buffered saline-Tween 20 (5% non-fat powdered milk buffered in Tris-HCl, pH 8.0, 150 mM NaCl and 0.05% Tween 20). Proteins were visualized by using enhanced chemiluminescence (Bio-Rad). To assess the presence of comparable amounts of proteins in each lane, the same membranes were stripped and probed with monoclonal mouse anti-alpha tubulin antibody (Abcam) followed by anti-mouse IgG (Sigma).

Clonogenic Assay

Single-cell suspensions of exponentially growing cultures (10^2, 3×10^2 and 10^3) were seeded into six-well plates pretreated with 0.1% gelatin. Following adherence (3–4 hrs post plating) cells were irradiated at the indicated doses and then incubated at 37°C for seven days. Following incubation, cells were fixed with formalin 2% and stained with Crystal violet (0.05% w/v). Colonies of > 20 cells (at least, 4 cells divisions) were counted by inverted microscope, at 4- to 10-fold magnification. Survival rate was calculated as a ratio between the numbers of colonies grown in each irradiation dose to the numbers of colonies grown in non-irradiated cultures.

Detection of DSBs by Flow cytometry

At time intervals, cells were collected, washed with PBS, fixed in ice-cold 1% methanol-free formaldehyde solution in PBS and stored in ice-cold 70% ethanol. Before analysis, the ethanol was aspirated, cells were rinsed in solution of 1% BSA, 0.2% Triton X-100 in PBS (BSA–T–PBS) and incubated overnight at 4°C with anti-γH2AX antibody (eBioscience). Following rinse, the cells were suspended in FITC-conjugated anti-mouse IgG antibody diluted in BSA–T–PBS for 1 hr in dark and 10^4 cells were analyzed by Eclipse flow Cytometer (iCYT). Analyses were performed with FCS Express 4 Research edition software.

Mass spectrometry analysis

Sample preparation: 100μl of cell lysate samples were denaturized using 8M urea followed by reduction and alkylation. The samples were overnight incubated with cold acetone

Author Manuscript Author Manuscript Author Manuscript Author Manuscript

followed by centrifugation, and the protein precipitates were collected and re-dissolved in 25mM ammonium bi-carbonate. Trypsin was added to the protein sample and incubated for overnight in 37° C. After the trypsinization process the peptides mixture was desalted on stage column, evaporated to dryness, and rehydrated with 10μl 1% Formic acid.

The peptides were re-suspended in 0.1% Formic acid, and 33% of sample volume were subjected to LC-MSMS analysis. The peptides were resolved by reverse-phase chromatography on 0.075 × 180-mm fused silica capillaries (J&W) packed with Reprosil reversed phase material (Dr. Maisch GmbH, Germany). The peptides were eluted with linear 180 minutes gradient of 5 to 28%, 15 minutes gradient of 28 to 95% and 25 minutes at 95% acetonitrile with 0.1% formic acid in water at flow rates of 0.15 μl/min. Mass spectrometry was performed by Q Exactive HFX mass spectrometer (Thermo) in a positive mode (m/z 350–1800, resolution 120,000 ion time 30) using repetitively full MS scan followed by collision induces dissociation (HCD) of the 15 most dominant ions selected from the first MS scan.

Data analysis was done by using PD 2.2 Software and database searches were performed against the Human UniProtKB/TrEMBL database using Sequest search engine. Analysis of the raw MS data was carried out using programs written in Matlab R2017a, and packages in PARTEK Genomic Suite 7.13.0402 were used for the principal component analysis (PCA). The MS and the data analysis methods were described before [45]

PCR amplification and next generation sequencing

Genomic DNA from cells was isolated 72 hrs after transfection with pCMV-NLS-I-Sce1, using EZ-DNA genomic DNA isolation reagent (Biological Industries). First PCR for performing the next generation sequencing (NGS) using 2μg of cellular genomic DNA served as a template for 131 bp flanking to the ISceI site using the following, primers with additional over hanged sequences (underlined):

Forward:
5’CGTCGGCAGCGTCAGATGTGTATAAGAGACAGGCCTCTGCTAACCATGTTCATGCC;

Reverse:
5’GTCTCGTGGGCTCGGAGATGTGTATAAGAGACAGCCAGGATGGGCACCACCCCGG.

PCR amplifications were performed as follows: 95°C for 3 min, 20 cycles of 95°C for 30s, 58°C for 30s, 72°C for 1 min, 72°C for 10 min. PCR products were purified by using PureLink Quick PCR purification Kit according to the manufacturer instructions and samples were submitted for NGS.

Library preparation and next generation sequencing details

The purified PCR products of EJ5 (5 μl) were subjected to a second round of amplification to assign unique index sequences (barcode) for each sample using Nextera XT Index Kit (Illumina, San Diego, CA, USA), 2x KAPA HiFi HotStart Ready Mix (25 μl), PCR Grade water (10 μl) in total reaction volume of 50μl. The following PCR program was used: 95°C

Author Manuscript Author Manuscript Author Manuscript Author Manuscript

for 3 minutes, followed with 8 cycles of 95°C for 30 seconds, 55°C for 30 seconds and 72°C for 30 seconds, then 72°C for 5 minutes and finally hold at 4°C. The product was purified by Agencourt AMPure XP system (X1) (A63881; Beckman Coulter Genomics), and eluted in 30 μl elution buffer. Library purity and quantity were evaluated by 4200 TapeStation System (Agilent Technologies, Inc., Santa Clara, CA, USA) using D1000 ScreenTape kit (Agilent) and by Qubit® Fluorometer (Invitrogen, Carlsbad, CA, USA) using Qubit dsDNA high-sensitivity assay (Invitrogen). Pool concentration of 4 nM was prepared and 1.5×10^6 or 3×10^5 reads for each sample were targeted. Samples were deep sequenced on NextSeq 500/550 machine using the 150-cycle Mid Output Kit (Illumina).

Sequencing data analysis

Fastq files (single-end 150bp long) were randomly down-sampled to an equal depth of 1.5×10^6 (first experiment), 3×10^5 (second experiment) and 10^5 (third experiment) reads per sample. Reads were filtered to include only those containing an exact match to the last 5 nucleotides of the forward primer sequence, within 3 nucleotides distance from its expected position (“usable reads”). These reads were clipped from the exact primer match to the end of the 150bp-long read, yielding sequences with variable lengths (depending on deletions or insertions in their sequence). In these sequences, the accurate repaired (original plasmid sequence) read length is 131 bp. The sequencing data was subjected to the Sequence Read Archive (SRA), BioProject accession number is PRJNA727730. Reads were then aligned to the corresponding fragment in the un-cleaved plasmid using the globalms function of the Biopython pair wise 2 module (parameters: match: 2, mismatch: -1, gap_open: -0.5, gap_extend: 0). Then, for each sample, the fraction of reads that perfectly align with the plasmid sequence, either along the entire fragment, or within the 18 bp long ISceI restriction site from the total usable reads was calculated. A repository with scripts used to analyze the sequencing data is available: https://github.com/erankotler/APOBEC3G_Britan-Rosich_et_al.

We note that while imperfect matches of sequencing reads to the reference plasmid sequence are comprised of inaccurate repairs of the formed DSBs and of sequencing errors, the latter is expected to be similar between samples within a given experiment (as these were processed and sequenced together, and down-sampled to the same sequencing depth) and therefore should not affect the results.

Supplementary Material

Refer to Web version on PubMed Central for supplementary material.

Acknowledgements

The authors thank David Ryan for assistance with the mouse breeding. We thank Dr. Idit Shiff from the Core Research Facility of the Hebrew University-Hadassah Medical School for the consultation and running the sequencing tasks. We thank Dr. Jeremy Stark for providing the pimEJ5GFP (EJ5) plasmid and for his useful discussions. Authors are grateful to Prof. Marc-Andre Langlois, Faculty of Medicine, University of Ottawa, Canada for providing us the A3G RNA binding mutants. Funding information: This work was supported by the following grants: The National Institute for Allergy and Infectious Disease (R01AI085015 to SRR), by The Joint Israel-Canada program (Grant No. 2665/16 MK), by The Milgrom Family Support Fund for projects in Military Medicine (4320614 MK) and partially by the Israel cancer association from the Abraham Rothstein fund (20200084 MK).

Author Manuscript Author Manuscript Author Manuscript Author Manuscript

Data availability:

Raw data were generated at the Core Department of the Hebrew University – Hadassah Medical School. Derived data supporting the findings of this study are available from the corresponding author M.K. on request.

Abbreviations

AID	Activation-induced deaminase
A3G	APOBEC3G
APOBEC	apolipoprotein B mRNA-editing enzyme-catalytic polypeptide-like
BER	base excision repair
CD	cytosine deaminase
CSR	class-switch recombination
DLBCL	diffuse Large B-cell lymphoma
DSB	double-strand break
HDR	homology-directed repair
HR	homologous recombination
INDEL	insertion/deletion
IR	ionizing radiation
KD	knock-down
mA3	mouse-APOBEC3
NER	nucleotide excision repair
NHEJ	non-homologous end joining
PBMC	peripheral blood mononuclear cells
PCA	principal components analysis
SH	somatic hypermutations
ssDNA	single-strand DNA
STRING	Search Tool for the Retrieval of Interacting Proteins
UNG	Uracil-DNA glycosidase

Author Manuscript Author Manuscript Author Manuscript Author Manuscript

References:

1. Jarmuz A, Chester A, Bayliss J, Gisbourne J, Dunham I, Scott J & Navaratnam N (2002) An anthropoid-specific locus of orphan C to U RNA-editing enzymes on chromosome 22, Genomics. 79, 285–96. [PubMed: 11863358]
2. Sawyer SL, Emerman M & Malik HS (2004) Ancient adaptive evolution of the primate antiviral DNA-editing enzyme APOBEC3G, PLoS Biol. 2, e275. [PubMed: 15269786]
3. Conticello SG (2008) The AID/APOBEC family of nucleic acid mutators, Genome Biol. 9, 1–10.
4. Harris RS & Dudley JP (2015) APOBECs and virus restriction, Virology. 479–480, 131–45.
5. Conticello SG, Thomas CJ, Petersen-Mahrt SK & Neuberger MS (2005) Evolution of the AID/APOBEC family of polynucleotide (deoxy) cytidine deaminases, Mol Biol Evol. 22, 367–377. [PubMed: 15496550]
6. Conticello SG, Langlois MA, Yang Z & Neuberger MS (2007) DNA deamination in immunity: AID in the context of its APOBEC relatives, Advances in immunology. 94, 37–73. [PubMed: 17560271]
7. Harris RS & Liddament MT (2004) Retroviral restriction by APOBEC proteins, Nature reviews Immunology. 4, 868–77.
8. LaRue RS, Jonsson SR, Silverstein KA, Lajoie M, Bertrand D, El-Mabrouk N, Hotzel I, Andresdottir V, Smith TP & Harris RS (2008) The artiodactyl APOBEC3 innate immune repertoire shows evidence for a multi-functional domain organization that existed in the ancestor of placental mammals, BMC molecular biology. 9, 104. [PubMed: 19017397]
9. Alexandrov LB, Nik-Zainal S, Wedge DC, Aparicio SA, Behjati S, Biankin AV, Bignell GR, Bolli N, Borg A, Borresen-Dale AL, Boyault S, Burkhardt B, Butler AP, Caldas C, Davies HR, Desmedt C, Eils R, Eyfjord JE, Foekens JA, Greaves M, Hosoda F, Hutter B, Ilicic T, Imbeaud S, Imielinski M, Jager N, Jones DT, Jones D, Knappskog S, Kool M, Lakhani SR, Lopez-Otin C, Martin S, Munshi NC, Nakamura H, Northcott PA, Pajic M, Papaemmanuil E, Paradiso A, Pearson JV, Puente XS, Raine K, Ramakrishna M, Richardson AL, Richter J, Rosenstiel P, Schlesner M, Schumacher TN, Span PN, Teague JW, Totoki Y, Tutt AN, Valdes-Mas R, van Buuren MM, van 't Veer L, Vincent-Salomon A, Waddell N, Yates LR, Zucman-Rossi J, Futreal PA, McDermott U, Lichter P, Meyerson M, Grimmond SM, Siebert R, Campo E, Shibata T, Pfister SM, Campbell PJ & Stratton MR (2013) Signatures of mutational processes in human cancer, Nature. 500, 415–21. [PubMed: 23945592]
10. Nik-Zainal S, Wedge DC, Alexandrov LB, Petljak M, Butler AP, Bolli N, Davies HR, Knappskog S, Martin S, Papaemmanuil E, Ramakrishna M, Shlien A, Simonic I, Xue Y, Tyler-Smith C, Campbell PJ & Stratton MR (2014) Association of a germline copy number polymorphism of APOBEC3A and APOBEC3B with burden of putative APOBEC-dependent mutations in breast cancer, Nature genetics. 46, 487–91. [PubMed: 24728294]
11. Taylor BJ, Nik-Zainal S, Wu YL, Stebbings LA, Raine K, Campbell PJ, Rada C, Stratton MR & Neuberger MS (2013) DNA deaminases induce break-associated mutation showers with implication of APOBEC3B and 3A in breast cancer kataegis, eLife. 2, e00534. [PubMed: 23599896]
12. Nik-Zainal S, Alexandrov LB, Wedge DC, Van Loo P, Greenman CD, Raine K, Jones D, Hinton J, Marshall J, Stebbings LA, Menzies A, Martin S, Leung K, Chen L, Leroy C, Ramakrishna M, Rance R, Lau KW, Mudie LJ, Varela I, McBride DJ, Bignell GR, Cooke SL, Shlien A, Gamble J, Whitmore I, Maddison M, Tarpey PS, Davies HR, Papaemmanuil E, Stephens PJ, McLaren S, Butler AP, Teague JW, Jonsson G, Garber JE, Silver D, Miron P, Fatima A, Boyault S, Langerod A, Tutt A, Martens JW, Aparicio SA, Borg A, Salomon AV, Thomas G, Borresen-Dale AL, Richardson AL, Neuberger MS, Futreal PA, Campbell PJ & Stratton MR (2012) Mutational processes molding the genomes of 21 breast cancers, Cell. 149, 979–93. [PubMed: 22608084]
13. Roberts SA & Gordenin DA (2014) Hypermutation in human cancer genomes: footprints and mechanisms, Nature Reviews Cancer. 14, 786–800. [PubMed: 25568919]
14. Schrader CE, Linehan EK, Mochegova SN, Woodland RT & Stavnezer J (2005) Inducible DNA breaks in Ig S regions are dependent on AID and UNG, The Journal of experimental medicine. 202, 561–8. [PubMed: 16103411]
15. Nik-Zainal S, Van Loo P, Wedge DC, Alexandrov LB, Greenman CD, Lau KW, Raine K, Jones D, Marshall J, Ramakrishna M, Shlien A, Cooke SL, Hinton J, Menzies A, Stebbings LA, Leroy

Author Manuscript Author Manuscript Author Manuscript Author Manuscript

C, Jia M, Rance R, Mudie LJ, Gamble SJ, Stephens PJ, McLaren S, Tarpey PS, Papaemmanuil E, Davies HR, Varela I, McBride DJ, Bignell GR, Leung K, Butler AP, Teague JW, Martin S, Jonsson G, Mariani O, Boyault S, Miron P, Fatima A, Langerod A, Aparicio SA, Tutt A, Sieuwerts AM, Borg A, Thomas G, Salomon AV, Richardson AL, Borresen-Dale AL, Futreal PA, Stratton MR & Campbell PJ (2012) The life history of 21 breast cancers, Cell. 149, 994–1007. [PubMed: 22608083]

16. Boichard A, Tsigelny IF & Kurzrock R (2017) High expression of PD-1 ligands is associated with kataegis mutational signature and APOBEC3 alterations, Oncoimmunology. 6, e1284719. [PubMed: 28405512]
17. Cannataro VL, Gaffney SG, Sasaki T, Issaeva N, Grewal NK, Grandis JR, Yarbrough WG, Burtness B, Anderson KS & Townsend JP (2019) APOBEC-induced mutations and their cancer effect size in head and neck squamous cell carcinoma, Oncogene. 38, 3475–3487. [PubMed: 30647454]
18. Gillison ML, Akagi K, Xiao W, Jiang B, Pickard RK, Li J, Swanson BJ, Agrawal AD, Zucker M & Stache-Crain B (2019) Human papillomavirus and the landscape of secondary genetic alterations in oral cancers, Genome Res. 29, 1–17. [PubMed: 30563911]
19. Burns MB, Temiz NA & Harris RS (2013) Evidence for APOBEC3B mutagenesis in multiple human cancers, Nature genetics. 45, 977–83. [PubMed: 23852168]
20. Burns MB, Lackey L, Carpenter MA, Rathore A, Land AM, Leonard B, Refsland EW, Kotandeniya D, Tretyakova N, Nikas JB, Yee D, Temiz NA, Donohue DE, McDougle RM, Brown WL, Law EK & Harris RS (2013) APOBEC3B is an enzymatic source of mutation in breast cancer, Nature. 494, 366–70. [PubMed: 23389445]
21. Law EK, Levin-Klein R, Jarvis MC, Kim H, Argyris PP, Carpenter MA, Starrett GJ, Temiz NA, Larson LK, Durfee C, Burns MB, Vogel RI, Stavrou S, Aguilera AN, Wagner S, Largaespada DA, Starr TK, Ross SR & Harris RS (2020) APOBEC3A catalyzes mutation and drives carcinogenesis in vivo, The Journal of experimental medicine. 217.
22. Helleday T, Eshtad S & Nik-Zainal S (2014) Mechanisms underlying mutational signatures in human cancers, Nature reviews Genetics. 15, 585–98.
23. Treger RS, Tokuyama M, Dong H, Salas-Briceno K, Ross SR, Kong Y & Iwasaki A (2019) Human APOBEC3G prevents emergence of infectious endogenous retrovirus in mice, J Virol. 93, e00728–19. [PubMed: 31341050]
24. Iwatani Y, Chan DS, Wang F, Maynard KS, Sugiura W, Gronenborn AM, Rouzina I, Williams MC, Musier-Forsyth K & Levin JG (2007) Deaminase-independent inhibition of HIV-1 reverse transcription by APOBEC3G, Nucleic acids research. 35, 7096–108. [PubMed: 17942420]
25. Schumacher AJ, Nissley DV & Harris RS (2005) APOBEC3G hypermutates genomic DNA and inhibits Ty1 retrotransposition in yeast, Proceedings of the National Academy of Sciences of the United States of America. 102, 9854–9. [PubMed: 16000409]
26. Bogerd HP, Wiegand HL, Hulme AE, Garcia-Perez JL, O'Shea KS, Moran JV & Cullen BR (2006) Cellular inhibitors of long interspersed element 1 and Alu retrotransposition, Proceedings of the National Academy of Sciences. 103, 8780–8785.
27. Harris RS, Hultquist JF & Evans DT (2012) The restriction factors of human immunodeficiency virus, The Journal of biological chemistry. 287, 40875–83. [PubMed: 23043100]
28. Liu MC, Liao WY, Buckley KM, Yang SY, Rast JP & Fugmann SD (2018) AID/APOBEC-like cytidine deaminases are ancient innate immune mediators in invertebrates, Nat Commun. 9, 1948. [PubMed: 29769532]
29. Roberts SA, Lawrence MS, Klimczak LJ, Grimm SA, Fargo D, Stojanov P, Kiezun A, Kryukov GV, Carter SL & Saksena G (2013) An APOBEC cytidine deaminase mutagenesis pattern is widespread in human cancers, Nature genetics. 45, 970–976. [PubMed: 23852170]
30. Mussil B, Sauermann U, Motzkus D, Stahl-Hennig C & Sopper S (2011) Increased APOBEC3G and APOBEC3F expression is associated with low viral load and prolonged survival in simian immunodeficiency virus infected rhesus monkeys, Retrovirology. 8, 77. [PubMed: 21955401]
31. Carpenter MA, Li M, Rathore A, Lackey L, Law EK, Land AM, Leonard B, Shandilya SM, Bohn MF, Schiffer CA, Brown WL & Harris RS (2012) Methylcytosine and normal cytosine

Author Manuscript Author Manuscript Author Manuscript Author Manuscript

deamination by the foreign DNA restriction enzyme APOBEC3A, The Journal of biological chemistry. 287, 34801–8. [PubMed: 22896697]

32. Suspene R, Aynaud M-M, Vartanian J-P & Wain-Hobson S (2013) Efficient deamination of 5-methylcytidine and 5-substituted cytidine residues in DNA by human APOBEC3A cytidine deaminase, PLoS One. 8, e63461. [PubMed: 23840298]
33. Schutsky EK, Nabel CS, Davis AK, DeNizio JE & Kohli RM (2017) APOBEC3A efficiently deaminates methylated, but not TET-oxidized, cytosine bases in DNA, Nucleic acids research. 45, 7655–7665. [PubMed: 28472485]
34. Stenglein MD, Burns MB, Li M, Lengyel J & Harris RS (2010) APOBEC3 proteins mediate the clearance of foreign DNA from human cells, Nat Struct Mol Biol. 17, 222. [PubMed: 20062055]
35. Niavarani A, Currie E, Reyal Y, Anjos-Afonso F, Horswell S, Griessinger E, Sardina JL & Bonnet D (2015) APOBEC3A is implicated in a novel class of G-to-A mRNA editing in WT1 transcripts, PLoS One. 10, e0120089. [PubMed: 25807502]
36. Sharma S, Patnaik SK, Taggart RT, Kannisto ED, Enriquez SM, Gollnick P & Baysal BE (2015) APOBEC3A cytidine deaminase induces RNA editing in monocytes and macrophages, Nat Commun. 6, 1–15.
37. Chen H, Lilley CE, Yu Q, Lee DV, Chou J, Narvaiza I, Landau NR & Weitzman MD (2006) APOBEC3A is a potent inhibitor of adeno-associated virus and retrotransposons, Current Biology. 16, 480–485. [PubMed: 16527742]
38. Stavrou S & Ross SR (2015) APOBEC3 proteins in viral immunity, The Journal of Immunology. 195, 4565–4570. [PubMed: 26546688]
39. Nowarski R, Wilner OI, Cheshin O, Shahar OD, Kenig E, Baraz L, Britan-Rosich E, Nagler A, Harris RS, Goldberg M, Willner I & Kotler M (2012) APOBEC3G enhances lymphoma cell radioresistance by promoting cytidine deaminase-dependent DNA repair, Blood. 120, 366–75. [PubMed: 22645179]
40. Jais J-P, Haioun C, Molina TJ, Rickman DS, De Reynies A, Berger F, Gisselbrecht C, Brière J, Reyes F & Gaulard P (2008) The expression of 16 genes related to the cell of origin and immune response predicts survival in elderly patients with diffuse large B-cell lymphoma treated with CHOP and rituximab, Leukemia. 22, 1917–1924. [PubMed: 18615101]
41. Tong Y, Kikuhara S, Onodera T, Chen L, Myat AB, Imamichi S, Sasaki Y, Murakami Y, Nozaki T, Fujimori H & Masutani M (2022) Radiosensitization to gamma-Ray by Functional Inhibition of APOBEC3G, International journal of molecular sciences. 23.
42. Wang Y, Wu S, Zheng S, Wang S, Wali A, Ezhilarasan R, Sulman EP, Koul D & Alfred Yung WK (2017) APOBEC3G acts as a therapeutic target in mesenchymal gliomas by sensitizing cells to radiation-induced cell death, Oncotarget. 8, 54285–54296. [PubMed: 28903341]
43. Prabhu P, Shandilya SM, Britan-Rosich E, Nagler A, Schiffer CA & Kotler M (2016) Inhibition of APOBEC3G activity impedes double-stranded DNA repair, The FEBS journal. 283, 112–29. [PubMed: 26460502]
44. Hultquist JF, Lengyel JA, Refsland EW, LaRue RS, Lackey L, Brown WL & Harris RS (2011) Human and rhesus APOBEC3D, APOBEC3F, APOBEC3G, and APOBEC3H demonstrate a conserved capacity to restrict Vif-deficient HIV-1, J Virol. 85, 11220–34. [PubMed: 21835787]
45. Botvinnik A, Shivam P, Smith Y, Sharma G, Olshevsky U, Moshel O, Manevitch Z, Climent N, Oliva H, Britan-Rosich E & Kotler M (2021) APOBEC3G rescues cells from the deleterious effects of DNA damage, The FEBS journal. 288, 6063–6077. [PubMed: 33999509]
46. Land AM, Law EK, Carpenter MA, Lackey L, Brown WL & Harris RS (2013) Endogenous APOBEC3A DNA cytosine deaminase is cytoplasmic and nongenotoxic, The Journal of biological chemistry. 288, 17253–60. [PubMed: 23640892]
47. Stavrou S, Crawford D, Blouch K, Browne EP, Kohli RM & Ross SR (2014) Different modes of retrovirus restriction by human APOBEC3A and APOBEC3G in vivo, PLoS pathogens. 10, e1004145. [PubMed: 24851906]
48. Cadena C, Stavrou S, Manzoni T, Iyer SS, Bibollet-Ruche F, Zhang W, Hahn BH, Browne EP & Ross SR (2016) The effect of HIV-1 Vif polymorphisms on A3G anti-viral activity in an in vivo mouse model, Retrovirology. 13, 45. [PubMed: 27363431]

Author Manuscript Author Manuscript Author Manuscript Author Manuscript

49. Okeoma CM, Lovsin N, Peterlin BM & Ross SR (2007) APOBEC3 inhibits mouse mammary tumour virus replication in vivo, Nature. 445, 927–930. [PubMed: 17259974]
50. Williams JP, Brown SL, Georges GE, Hauer-Jensen M, Hill RP, Huser AK, Kirsch DG, MacVittie TJ, Mason KA & Medhora MM (2010) Animal models for medical countermeasures to radiation exposure, Radiat Res. 173, 557–578. [PubMed: 20334528]
51. Shindo K, Li M, Gross PJ, Brown WL, Harjes E, Lu Y, Matsuo H & Harris RS (2012) A comparison of two single-stranded DNA binding models by mutational analysis of APOBEC3G, Biology. 1, 260–276. [PubMed: 24832226]
52. Bennardo N, Cheng A, Huang N & Stark JM (2008) Alternative-NHEJ is a mechanistically distinct pathway of mammalian chromosome break repair, PLoS genetics. 4, e1000110. [PubMed: 18584027]
53. Belanger K, Savoie M, Rosales Gerpe MC, Couture JF & Langlois MA (2013) Binding of RNA by APOBEC3G controls deamination-independent restriction of retroviruses, Nucleic acids research. 41, 7438–52. [PubMed: 23761443]
54. Chiu YL, Witkowska HE, Hall SC, Santiago M, Soros VB, Esnault C, Heidmann T & Greene WC (2006) High-molecular-mass APOBEC3G complexes restrict Alu retrotransposition, Proceedings of the National Academy of Sciences of the United States of America. 103, 15588–93. [PubMed: 17030807]
55. Opi S, Takeuchi H, Kao S, Khan MA, Miyagi E, Goila-Gaur R, Iwatani Y, Levin JG & Strebel K (2006) Monomeric APOBEC3G is catalytically active and has antiviral activity, J Virol. 80, 4673–82. [PubMed: 16641260]
56. Nowarski R, Britan-Rosich E, Shiloach T & Kotler M (2008) Hypermutation by intersegmental transfer of APOBEC3G cytidine deaminase, Nat Struct Mol Biol. 15, 1059–66. [PubMed: 18820687]
57. Stavrou S, Zhao W, Blouch K & Ross SR (2018) Deaminase-Dead Mouse APOBEC3 Is an In Vivo Retroviral Restriction Factor, J Virol. 92.
58. Koning FA, Newman EN, Kim E-Y, Kunstman KJ, Wolinsky SM & Malim MH (2009) Defining APOBEC3 expression patterns in human tissues and hematopoietic cell subsets, J Virol. 83, 9474–9485. [PubMed: 19587057]
59. Weinstock DM, Nakanishi K, Helgadottir HR & Jasin M (2006) Assaying double-strand break repair pathway choice in mammalian cells using a targeted endonuclease or the RAG recombinase, Methods Enzymol. 409, 524–540. [PubMed: 16793422]
60. Scully R, Panday A, Elango R & Willis NA (2019) DNA double-strand break repair-pathway choice in somatic mammalian cells, Nature reviews Molecular cell biology. 20, 698–714. [PubMed: 31263220]
61. Nowarski R, Prabhu P, Kenig E, Smith Y, Britan-Rosich E & Kotler M (2014) APOBEC3G inhibits HIV-1 RNA elongation by inactivating the viral trans-activation response element, Journal of molecular biology. 426, 2840–53. [PubMed: 24859335]
62. Morse M, Naufer MN, Feng Y, Chelico L, Rouzina I & Williams MC (2019) HIV restriction factor APOBEC3G binds in multiple steps and conformations to search and deaminate single-stranded DNA, eLife. 8, e52649. [PubMed: 31850845]
63. Pinto Y, Gabay O, Arbiza L, Sams AJ, Keinan A & Levanon EY (2016) Clustered mutations in hominid genome evolution are consistent with APOBEC3G enzymatic activity, Genome Res. 26, 579–587. [PubMed: 27056836]
64. Conner KL, Shaik AN, Marshall KA, Floyd AM, Ekinci E, Lindquist J, Sawant A, Lei W, Adolph MB & Chelico L (2020) APOBEC3 enzymes mediate efficacy of cisplatin and are epistatic with base excision repair and mismatch repair in platinum response, NAR cancer. 2, zcaa033. [PubMed: 33196045]
65. Oliva H, Pacheco R, Martinez-Navio JM, Rodriguez-Garcia M, Naranjo-Gomez M, Climent N, Prado C, Gil C, Plana M, Garcia F, Miro JM, Franco R, Borras FE, Navaratnam N, Gatell JM & Gallart T (2016) Increased expression with differential subcellular location of cytidine deaminase APOBEC3G in human CD4(+) T-cell activation and dendritic cell maturation, Immunol Cell Biol. 94, 689–700. [PubMed: 26987686]

Author Manuscript Author Manuscript Author Manuscript Author Manuscript

66. Liu W, Newhall KP, Khani F, Barlow L, Nguyen D, Gu L, Eng K, Bhinder B, Uppal M, Récapet C, Sboner A, Ross SR, Elemento O, Chelico L & Faltas BM (2022) The cytidine deaminase APOBEC3G drives cancer mutagenesis and clonal evolution in bladder cancer, bioRxiv, 2022.09.05.503899.

67. Bhargava R, Onyango DO & Stark JM (2016) Regulation of single-strand annealing and its role in genome maintenance, Trends in Genetics. 32, 566–575. [PubMed: 27450436]

68. De Laat WL, Appeldoorn E, Sugasawa K, Weterings E, Jaspers NG & Hoeijmakers JH (1998) DNA-binding polarity of human replication protein A positions nucleases in nucleotide excision repair, Genes Dev. 12, 2598–2609. [PubMed: 9716411]

69. Al-Minawi AZ, Saleh-Gohari N & Helleday T (2008) The ERCC1/XPF endonuclease is required for efficient single-strand annealing and gene conversion in mammalian cells, Nucleic acids research. 36, 1–9. [PubMed: 17962301]

70. Gasior SL, Roy-Engel AM & Deininger PL (2008) ERCC1/XPF limits L1 retrotransposition, DNA Repair (Amst). 7, 983–989. [PubMed: 18396111]

71. Li S, Lu H, Wang Z, Hu Q, Wang H, Xiang R, Chiba T & Wu X (2019) ERCC1/XPF is important for repair of DNA double-strand breaks containing secondary structures, Iscience. 16, 63–78. [PubMed: 31153042]

72. Nilsen H, Rosewell I, Robins P, Skjelbred CF, Andersen S, Slupphaug G, Daly G, Krokan HE, Lindahl T & Barnes DE (2000) Uracil-DNA glycosylase (UNG)-deficient mice reveal a primary role of the enzyme during DNA replication, Mol Cell. 5, 1059–1065. [PubMed: 10912000]

73. Pearl LH (2000) Structure and function in the uracil-DNA glycosylase superfamily, Mutation Research/DNA Repair. 460, 165–181. [PubMed: 10946227]

74. Burgess JT, Rose M, Boucher D, Plowman J, Molloy C, Fisher M, O'Leary C, Richard DJ, O'Byrne KJ & Bolderson E (2020) The Therapeutic Potential of DNA Damage Repair Pathways and Genomic Stability in Lung Cancer, Front Oncol. 10, 1256. [PubMed: 32850380]

75. Nowarski R & Kotler M (2013) APOBEC3 Cytidine Deaminases in Double-Strand DNA Break Repair and Cancer Promotion, Cancer research. 73, 3494–8. [PubMed: 23598277]

76. Abu-Zhayia ER, Awwad SW, Ben-Oz BM, Khoury-Haddad H & Ayoub N (2018) CDYL1 fosters double-strand break-induced transcription silencing and promotes homology-directed repair, Journal of molecular cell biology. 10, 341–357. [PubMed: 29177481]

Author Manuscript
Author Manuscript
Author Manuscript
Author Manuscript

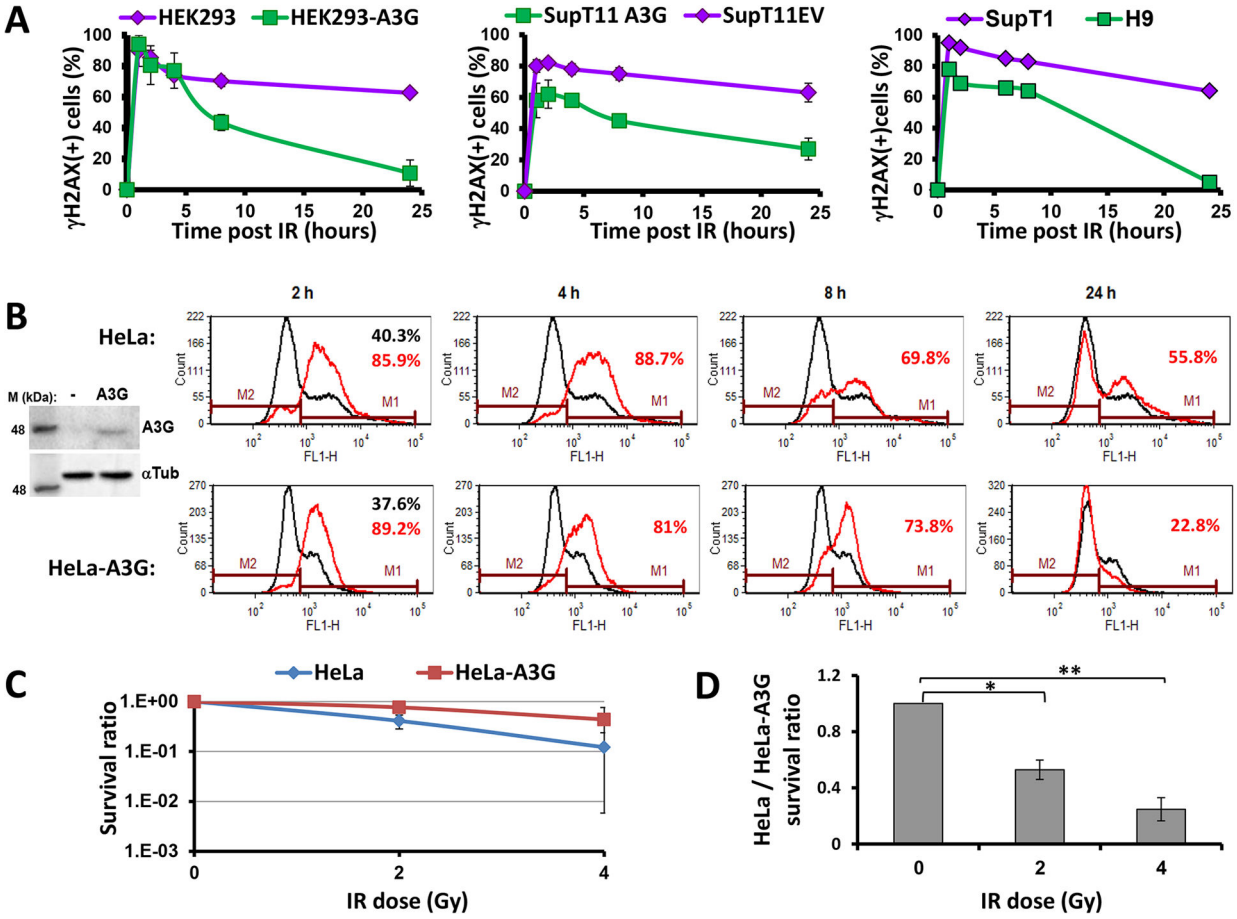

Figure 1. A3G promotes the repair of DSBs induced by IR in cultured cells:

(A) From left to right: HEK293 vs HEK293-A3G cells; SupT11A3G vs SupT11EV and H9 vs SupT1 cells were exposed to 3 Gy of ionizing radiation (IR). At the indicated times post irradiation cells were fixed, stained with anti γH2AX antibody, and analyzed by flow cytometry. Results represent the percentage of γH2AX-positive cells; each value represents the average of two or three independent experiments, ±standard deviation (SD). Statistical significance by two-tailed two-sample *t* test for HEK293/HEK293-A3G: p=0.051, p=0.026 8h and 24h, and for SupT11EV/A3G: p=0.02, p=0.014, p=0.03 for 4h, 8h and 24h. (**B):** A3G expression was confirmed by western blotting using anti-A3G C-terminus rabbit polyclonal antibody followed by detection with enhanced chemiluminescence (ECL). Mouse anti-α-Tubulin antibody was used as a loading control. Flow cytometry histograms of γH2AX-stained the 4 Gy-irradiated HeLa and HeLa-A3G cells are presented. Time points after IR exposure are indicated. Red curves – irradiated cells; black curves – non-irradiated control cells. Marker boundary is set on the intersection of the control and the irradiated sample curves. The percentage of γH2AX-positive cells is indicated. Ten thousands cells were assessed in each sample; (**C-D**) Clonogenic assay of irradiated HeLa and HeLa-A3G cells is shown. Briefly, cells were seeded at low density in 6-well plates 3 hours prior to IR exposure (2 and 4 Gy). Seven to nine days post irradiation cells were fixed, stained by Crystal Violet (0.05%) and colonies with >20 cells were counted. Survival rates are plotted in (**C**) and a ratio between the survival rates of HeLa vs HeLa-A3G in each IR dose

Author Manuscript Author Manuscript Author Manuscript Author Manuscript

is plotted in (**D**). Average of two independent experiments is presented, ±SD. Statistical significance: *, P<0.05; **, P<0.01 by two-tailed two-sample *t* test.

Author Manuscript Author Manuscript Author Manuscript Author Manuscript

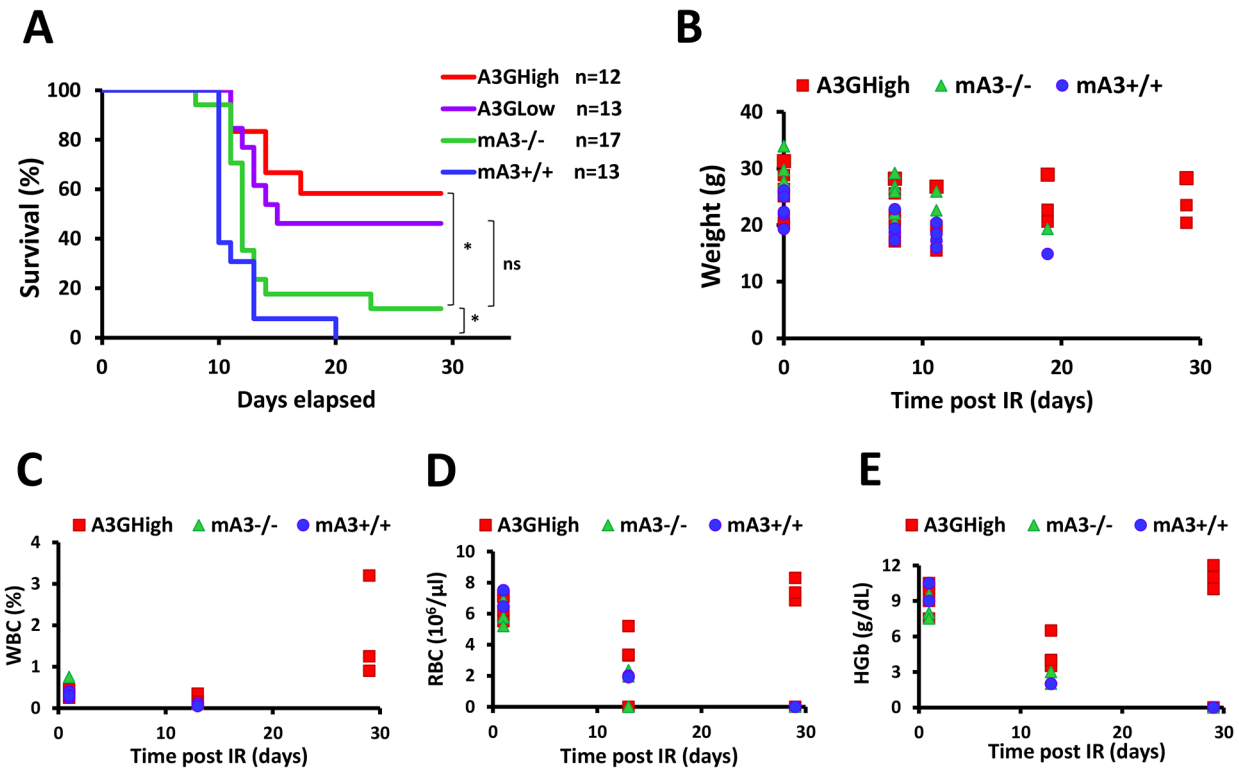

Figure 2. A3G rescues mice from IR-induced damage:

One-month old mice were whole body irradiated (8.25 Gy). Percentage of mice survival for each genotype group during 30 days post irradiation was determined. (**A)** Kaplan–Meier survival curves of mA3-competent mice (mA3+/+); the mA3 knocked-out (KO) mice (mA3−/−); the $A3G^{High}$ and $A3G^{Low}$ transgenic mice are shown. Genotype groups contained both female and male mice, as follows: mA3+/+ - 5 female and 8 male mice; mA3−/− - 10 female and 7 male mice; $A3G^{High}$ – 5 female and 7 male mice; $A3G^{Low}$ – 5 female and 8 male mice. Statistical significance: *, $P<0.05$, by one-sided two-sample *t* test; ns – not significant. **(B)** Body weight; **(C)** White blood cell count; **(D)** Red blood cell count and (**E)** Hemoglobin concentration are shown. **(B-E)** plots represent the results from one out of three independent experiments performed in the same conditions.

Author Manuscript Author Manuscript Author Manuscript Author Manuscript

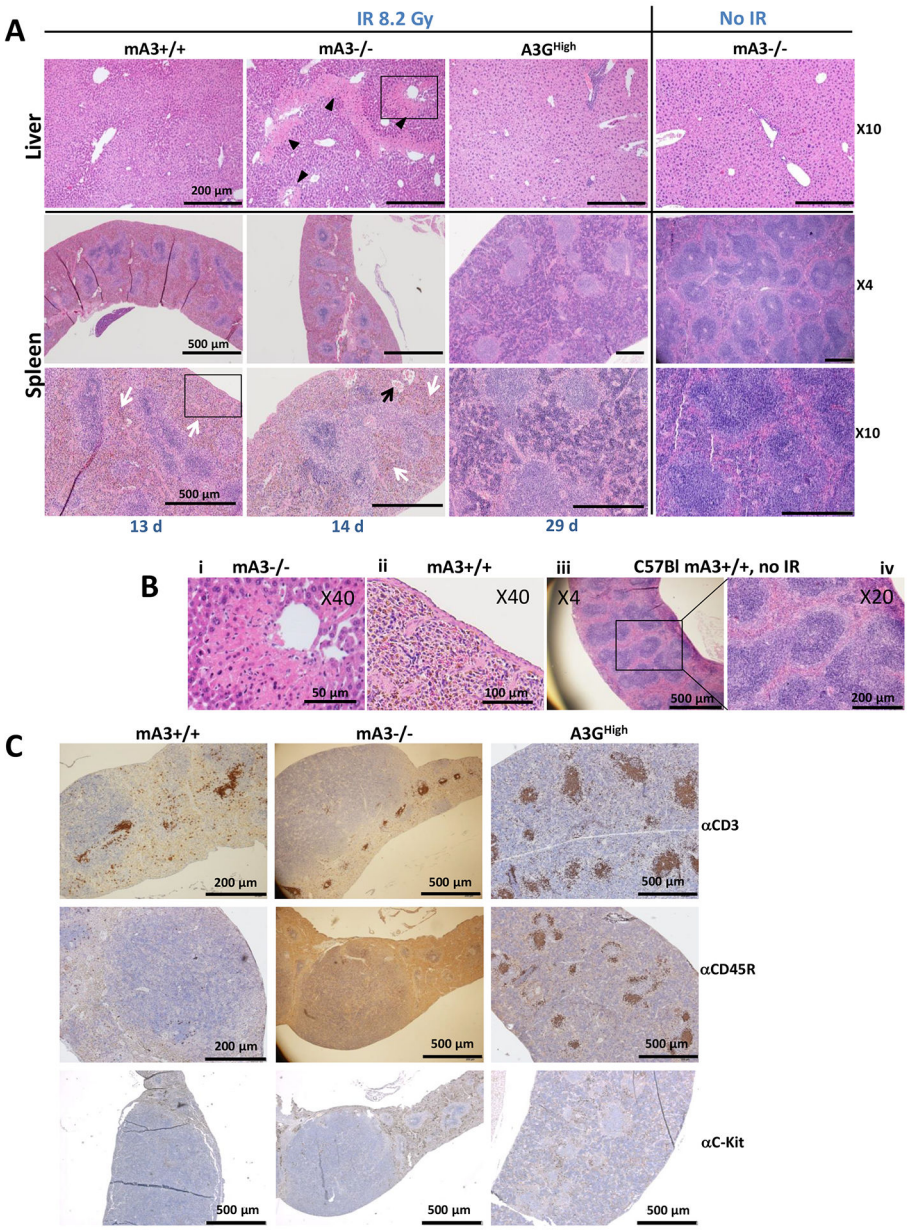

Figure 3. Histological examination of livers and spleens derived from the irradiated mice: **(A)** Livers (upper row) and spleens derived from 8.25 Gy-irradiated (first three columns) and non-irradiated (right column) mice are shown in photomicrographs. Samples in each column were prepared from the same mouse. Each sample represents its genotype group. Sizes of each genotype group are: n=7 for A3G^{High} +/+ (only mice survived the entire experiment were analyzed); n=17 for mA3−/−; n=13 for mA3+/+. Enlarged frames from mA3−/− liver and mA3+/+ spleen are shown in (**B i**) and (**B ii**), respectively. Spleen from non-irradiated C57BL mice (control) is presented (**B iii**) and (**B iv**). Organ-sections were stained with Hematoxylin and Eosin (H&E). Mice survival post irradiation is indicated. Scale-bars are indicated in (A): 200 µm (liver, upper row), 500 µm (spleen, middle and lower rows). Arrows indicate: necrosis (black triangles, liver sections), hemorrhage (black

Author Manuscript Author Manuscript Author Manuscript Author Manuscript

arrow, spleen) and brown-colored hemosiderin deposits (white arrows, spleen). (**C)** Spleen sections are stained with antibodies against CD3, B220 and c-Kit markers. Mice genotypes are indicated. Samples in each column were prepared from the same mouse. Scale-bars are indicated.

Author Manuscript Author Manuscript Author Manuscript Author Manuscript

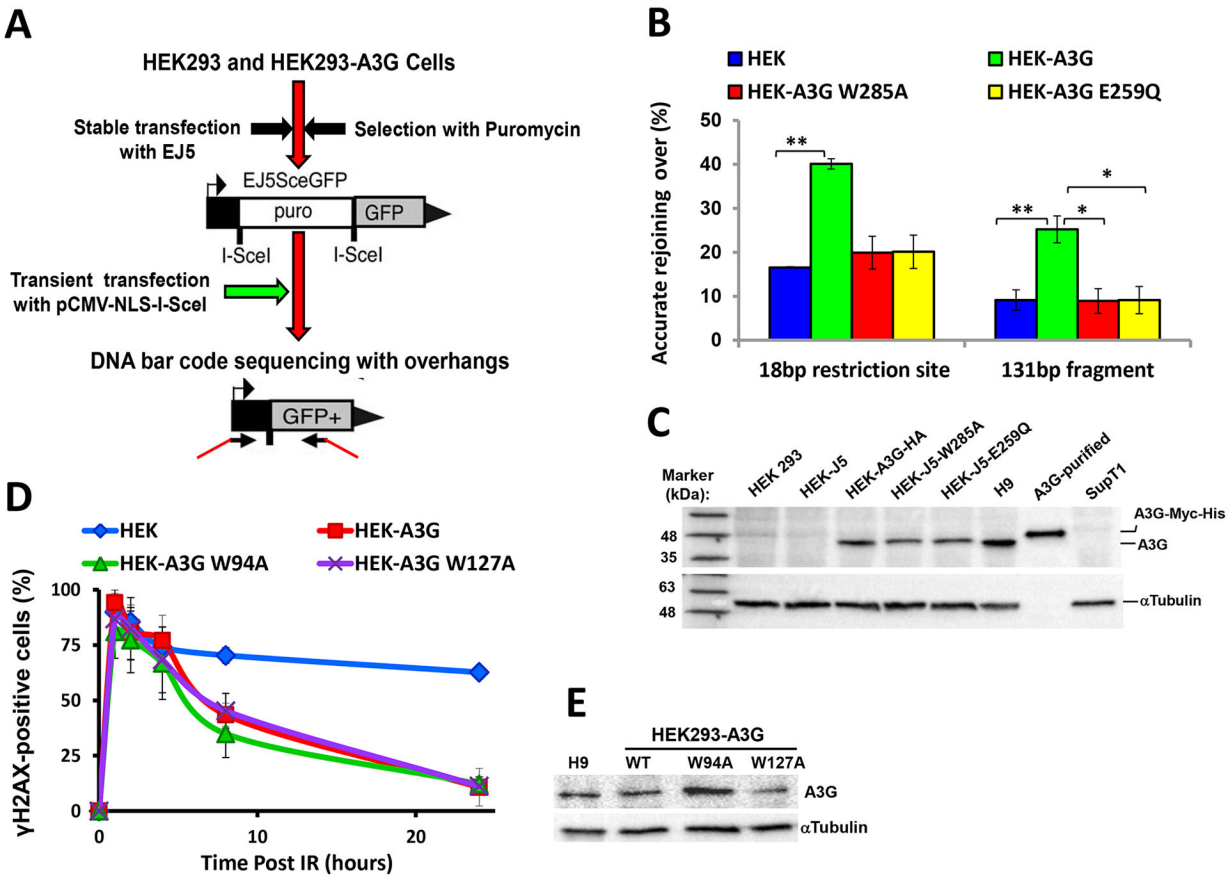

Figure 4. A3G promotes accurate DSB repair independently of RNA binding:

(A) Scheme describes the working-flow for preparation the 131nt fragments used for sequencing analyses. **(B)** Plot represents fractions of accurate rejoining over total reads calculated for the whole 131 bp fragment and for 18 bp ISceI restriction site, in HEK293, HEK293-A3G, HEK293-A3G-W285A and HEK293-A3G-E259Q cells (for details see Table 1 and Figure S1). Each value represents the average of three independent experiments, ±SD. Statistical significance: *, P<0.05; ** P<0.01 by two-tailed paired *t* test. **(C)** Western blots analysis of HEK293 cells transfected with WT or deamination-deficient mutants. Blots were probed with anti-A3G C-terminus antibody and anti-α-Tubulin HRP-conjugated antibody followed by detection with ECL. (**D)** HEK293 cells were stably transfected with WT A3G and with the RNA-binding mutants (W94A and W127A). Cells were irradiated with IR (3Gy), followed by incubation for the indicated time intervals and then stained with anti-γH2AX antibody and analyzed by flow cytometry. Plot shows the percentage of γH2AX-positive cells, as analyzed by flow cytometry. Each value represents the average of two independent experiments, ±SD. **(E)** Western blots analysis of HEK293 cells transfected with WT or with RNA binding-impaired A3G mutants. Blots were probed with anti-A3G C-terminus antibody, as described in **C**.

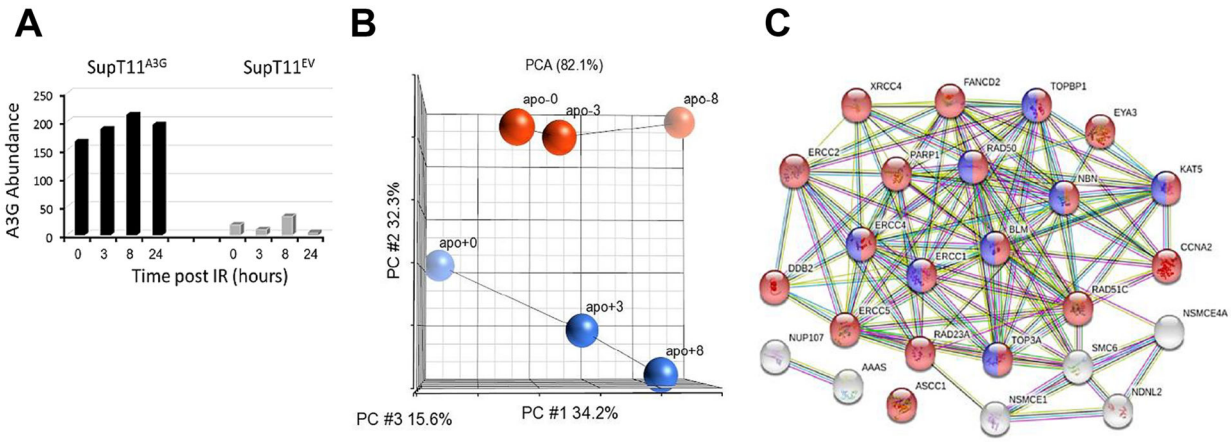

Figure 5. Proteomic analysis of the cellular proteins expressed in association with A3G:
(A) A3G protein content is shown in SupT11^{A3G} and SupT11^{EV} cells at the indicated time intervals after irradiation (4Gy), as identified by MS. **(B)** Principal component analysis (PCA) was performed on raw Mass Spec (MS) data from irradiated SupT11^{A3G} cells (blue balls) and SupT11^{EV} cells (red balls) at time points 0, 3 and 8 hours post-radiation. Presented is one of two independent experiments. **(C)** Interaction network of the 25 proteins as they appear in STRING database. Red color indicates the DNA Repair, while blue color refers to the HDR through Single-Strand Annealing (SSA) pathway, the most statistically significant enriched proteins pathways shown in Table 2 (for details see Results section). The connections between the genes are based on STRING evidence relating to active interaction sources, as co-expression, gene fusion, co-occurrence, neighborhood etc. For details see Supporting Information section (Table S1).

Author Manuscript Author Manuscript Author Manuscript Author Manuscript

Author Manuscript Author Manuscript Author Manuscript Author Manuscript

Table 1:

Analysis of the rejoining at the 131 bp fragment flanking the ISceI restriction site

Sample	Total reads	Usable reads	Usable read fraction	Accurate cleavage site (TAGGGATAACAGGGTAAT)	Inaccurate cleavage site	Fraction accurate over 18bp restriction site	Accurate over 131bp fragment	Fraction accurate over 131bp fragment
Exp#1								
HEK 293	1500000	1489717	0.993144667	245597	1244120	0.164861514	147287	0.098869114
HEK-A3G	1500000	1490608	0.993738667	600298	890310	0.402720232	374252	0.251073388
HEK-A3G-W285A	1500000	1491078	0.994052	336242	1154836	0.225502623	162888	0.10924177
HEK-A3G-E259Q	1500000	1490928	0.993952	339932	1150996	0.228000279	169167	0.113464232
Exp#2								
HEK 293	300000	299360	0.997866667	49263	250097	0.164561064	33043	0.110378808
HEK-A3G	300000	299389	0.997963333	123194	176195	0.411484724	84790	0.283210138
Exp#3								
HEK 293	100000	98643	0.98643	16514	82129	0.167411778	6456	0.065448131
HEK-A3G	100000	98601	0.98601	38315	60286	0.388586323	21886	0.221965294
HEK-A3G-W285A	100000	98578	0.98578	17048	81530	0.172939195	6844	0.069427256
HEK-A3G-E259Q	100000	98696	0.98696	17224	81472	0.174515685	6857	0.069475967

Author Manuscript Author Manuscript Author Manuscript Author Manuscript

Table 2:

The pathways including the most significantly expressed proteins selected by the STRING and REACTOM Databases

ID number	Pathway description	Observed gene count	Background gene count	False discovery rate	Matching proteins in your network (labels)
HSA-5685938	HDR through Single Strand Annealing (SSA)	8	36	7.27E-05	BLM, ERCC1,ERCC4, KAT5, NBN, RAD50, TOP3A, TOPBP1
HSA-73894	DNA Repair	19	290	7.27E-05	ASCC1, BLM, CCNA2, DDB2, ERCC1, ERCC2, ERCC4, ERCC5, EYA3, FANCD2, KAT5, NBN, PARP1, RAD23A, RAD50, RAD51C, TOP3A, TOPBP1, XRCC4
HSA-5693532	DNA Double-Strand Break Repair	13	147	1.10E-04	BLM, CCNA2, ERCC1, ERCC4, EYA3, KAT5, NBN, PARP1, RAD50, RAD51C, TOP3A, TOPBP1, XRCC4
HSA-3108214	SUMOylation of DNA damage response and repair proteins	9	69	2.50E-04	AAAS, BLM, NDNL2, NSMCE1, NSMCE4A, NUP107, PARP1, SMC6, XRCC4
HSA-5693538	Homology Directed Repair	11	119	3.20E-04	BLM, CCNA2, ERCC1, ERCC4, KAT5, NBN, PARP1, RAD50, RAD51C, TOP3A, TOPBP1
HSA-5693616	Presynaptic phase of homologous DNA pairing and strand exchange	7	38	3.50E-04	BLM, KAT5, NBN, RAD50, RAD51C, TOP3A, TOPBP1
HSA-5693554	Resolution of D-loop Structures through Synthesis-Dependent Strand Annealing (SDSA)	6	25	4.20E-04	BLM, KAT5, NBN, RAD50, RAD51C, TOP3A
HSA-5696395	Formation of Incision Complex in GG-NER	7	42	4.40E-04	DDB2, ERCC1, ERCC2, ERCC4, ERCC5, PARP1, RAD23A
HSA-3700989	Transcriptional Regulation by TP53	18	359	5.30E-04	BANP, BLM, CCNA2, CDK13, CNOT7, COX11, DDB2, ERCC2, FANCD2, KAT5, MAPK14, NBN, NELFB, PIP4K2C, RAD50, TAF13, TOP3A, TOPBP1
HSA-5693567	HDR through Homologous Recombination (HRR) or Single Strand Annealing (SSA)	10	113	6.10E-04	BLM, CCNA2, ERCC1, ERCC4, KAT5, NBN, RAD50, RAD51C, TOP3A, TOPBP1